Chemistry–A European Journal

Research Article
doi.org/10.1002/chem.202202082

Chemistry Europe
European Chemical Societies Publishing

www.chemeurj.org

Special Collection

A Macrocyclic Furan with Accessible Oxidation States: Switching Between Aromatic and Antiaromatic Global Ring Currents

Or Dishi,[a] Yuval Rahav,[a] Raanan Carmieli,[b] and Ori Gidron*[a]

In memory of François Diederich

Abstract: Macrocyclic furans are predicted to switch between global aromaticity and antiaromaticity, depending on their oxidation states. However, the macrocyclic furans reported to date are stabilized by electron withdrawing groups, which result in inaccessible oxidation states. To circumvent this problem, a post-macrocyclization approach was applied to introduce methylene-substituted macrocyclic furans, which display an extremely low oxidation potential of −0.23 vs. Fc/Fc$^+$, and are partially oxidized in ambient conditions. Additional oxidation to the dication results in aromaticity switching to a global 30πe^- aromatic state, as indicated by the formation of a strong diatropic current observed in the ^{1}H NMR spectrum. NICS and ACID calculations support this trend and provide evidence for a different pathway for the global current in the neutral and dicationic states. According to these findings, macrocyclic furans can be rendered as promising *p*-type materials with stable oxidation states.

Introduction

The inclusion of π-conjugated macrocycles as active electrode materials for batteries or *p*-type semiconductors largely depends on the existence of accessible oxidation states.[1–8] This can be governed by the interplay between local and global aromaticity.[9] While this interplay is commonly observed in macrocycles bearing porphyrins,[10] and other methine-spaced macrocycles, it is not commonly observed in α,α′-connected macrocycles,[11] for which local aromaticity is often the dominant factor.[11–17]

One example of such macrocycles is α,α′-macrocyclic thiophenes (**C$_n$T**, Scheme 1), first introduced by Bäuerle.[18–25] Theoretically, the 4*n*π-electron backbone should result in global antiaromaticity, but small macrocyclic thiophenes tend to deviate from planarity and exhibit a significant local aromatic character.[26]

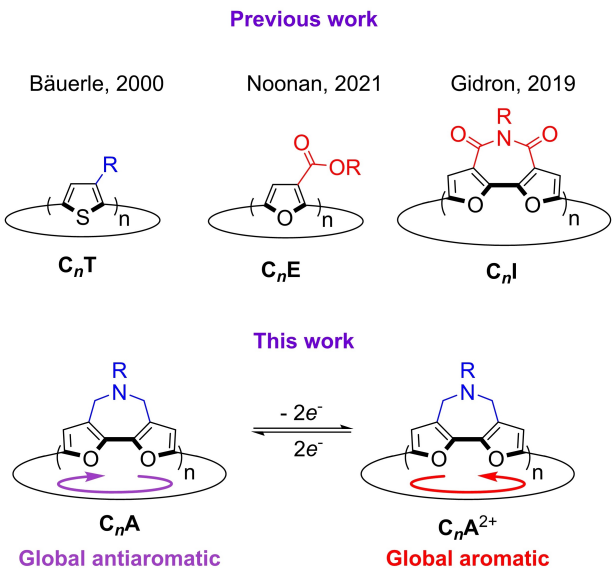

Scheme 1. Structures of cyclic α,α′-oligothiophenes (**C$_n$T**), macrocyclic oligofurans previously reported (**C$_n$I** and **C$_n$E**) and the α,α′-oligofurans discussed in this work (**C$_n$A**). R = alkyl. Red denotes electron withdrawing groups and blue denotes electron donating groups.

We previously reported that linear furan oligomers are more planar, exhibit a stronger quinoid (lower aromatic) character, and a lower oxidation potentials compared with their thiophene analogs.[27–30] Following this work, we predicted that small macrocyclic α-oligofurans consisting of 6–8 units should be

[a] O. Dishi, Y. Rahav, Prof. O. Gidron
Institute of Chemistry
The Hebrew University of Jerusalem
Edmond J. Safra Campus
Jerusalem 9190401 (Israel)
E-mail: ori.gidron@mail.huji.ac.il
Homepage: http://chem.ch.huji.ac.il/gidron/

[b] Dr. R. Carmieli
Chemical Research Support Unit,
Weizmann Institute of Science
Rehovot 7610001 (Israel)

Supporting information for this article is available on the WWW under https://doi.org/10.1002/chem.202202082

This publication is part of a Special Collection on aromatic chemistry in collaboration with the "19th International Symposium on Novel Aromatic Compounds (ISNA-19)".

planar, exhibit strong quinoid character, and high HOMO levels, rendering them as ideal *p*-type materials.[26] Having previously introduced the 2,2′-bifuran-3,3′-dicarboximide as a stable furan-based building block,[31] we reported a series of α,α′-oligofuran macrocycles (**C$_n$I**, Scheme 1).[32,33] Macrocyclic oligofurans consisting of ester-substituted groups were also recently reported by Noonan (**C$_n$E**, Scheme 1).[34] We have found that in contrast to most reported macrocyclic systems, **C$_n$I** exhibit a global antiaromatic character, which can explain their deviation from planarity with increasing size.[33]

Although the imide and ester groups stabilize the furan intermediates throughout the synthetic procedure, they reduce the electron density from the π-conjugated system, thus suppressing global ring current that stems from electron delocalization along the π-conjugated backbone. In addition, they significantly increase the oxidation potential, rendering the cation radical and dication species inaccessible.

It was thus clear that in order to account for global effects, as well as to access different oxidation states, the imide group must be replaced by groups such as alkyl, which cannot participate in the resonance of the π-conjugated backbone. However, since the high HOMO level of furan intermediates renders them unstable throughout the synthetic procedure, we found that a previous strategy applied to macrocyclic thiophenes and pyrroles, namely, the macrocyclization of β-alkyl-monomers,[35] is not applicable for furan analogs. We therefore postulated that the reduction of the imide group (which stabilize the intermediates) to amine should be performed post-macrocyclization.[36,37]

Herein we apply a post-macrocyclization approach to introduce the first macrocyclic oligofuran with no electron withdrawing groups, by reducing four imide groups to amines in a single step to yield **C$_4$A** (Scheme 1). We found that reducing the imide groups increases the global antiaromatic nature of the macrocycle in the neutral state. Unlike previous macrocyclic furans, the first and second oxidation states of **C$_4$A** are accessible both chemically and electrochemically, yielding polaron and bipolaron species, respectively. Oxidation involves switching from global antiaromaticity to global aromaticity, as observed experimentally and supported by calculations based on magnetic criteria.[38] To the best of our knowledge, the HOMO level of this macrocycle is higher than that of any π-conjugated macrocycle to-date.[18,21,39]

Results and Discussion

We have previously observed that long oligofurans readily undergo decomposition in solution under ambient conditions.[27] Indeed, attempts to reduce one unit of 2,2′-bifuran-3,3′-dicarboximide to a 2,2′-bifuran-3,3′-dimethylamine resulted in a product with low stability, which is likely to decompose along the synthetic pathway. We therefore decided to pursue the synthesis with the stable imide precursor, and reduce the macrocyclic **C$_4$I**, which was prepared as described previously.[32,33] The reduction of four imide groups to amines was performed by a slow addition of **C$_4$I** in THF to a suspension containing excess of lithium aluminum hydride ($LiAlH_4$) in THF at 0 °C, followed by gradual warming to room temperature to afford **C$_4$A** in 29% yield (Scheme 2). The macrocycle was characterized using NMR and MALDI-TOF (see the Supporting Information). To account for the global ring currents as detailed below, we have also synthesized the biphenyl-capped linear analogs (**(L$_1$I)Ph$_2$** and **(L$_1$A)Ph$_2$**, Scheme 2), by applying Suzuki coupling followed by reduction of the imide unit.

Linear oligofurans exhibit higher HOMO energies compared with thiophenes, by ca. 0.3 eV, rendering them as good *p*-type materials.[27] Our previous calculations predicted that for a furan macrocycle containing eight furan rings (which is analogous to **C$_4$A**), there should be a significantly larger difference, with a 0.6 eV higher HOMO level, compared with their thiophene analogs (-4.52 eV and −5.12 eV for macrocyclic octafuran and octatiophene, resectively).[26] The electron-donating -CH_2-NR-CH_2- in **C$_4$A** further increase the calculated HOMO level to −4.08 eV, which should render it as a very strong donor. The calculated HOMO level is 1.8 eV higher than that of the imide precursor **C$_4$I**, which should constitute a significant increase in the ring current.[33]

Cyclic voltammetry (CV) of **C$_4$A** shows two reversible oxidation peaks at −0.23 V (E_{ox}^1) and −0.04 V (E_{ox}^2) vs. Fc/Fc^+; no reduction peaks were observed (Figure 1). The first oxidation peak corresponds to a HOMO level of −4.57 eV, and the absence of a reduction peak can be rationalized based on the calculated energy for the LUMO level, −1.7 eV, which would place it beyond the electrochemical window of dichloromethane. For comparison, **C$_4$I** displayed only one oxidation peak at 0.78 V vs. Fc/Fc^+ (1 eV higher than **C$_4$A**). While some quinoid compounds such as tetrathiafulvalene derivatives[40] display low oxidation potential, aromatic materials with such low potentials are rare. Although the oxidation potential of a macrocyclic thiophene analog consisting of eight thiophene rings was not reported, the first oxidation potential of the larger derivative, **C$_{10}$T**, is ca. 0.3 V higher.[24] To the best of our knowledge, **C$_4$A** constitutes the lowest oxidation potential reported for π-conjugated macrocycles, and it is even lower

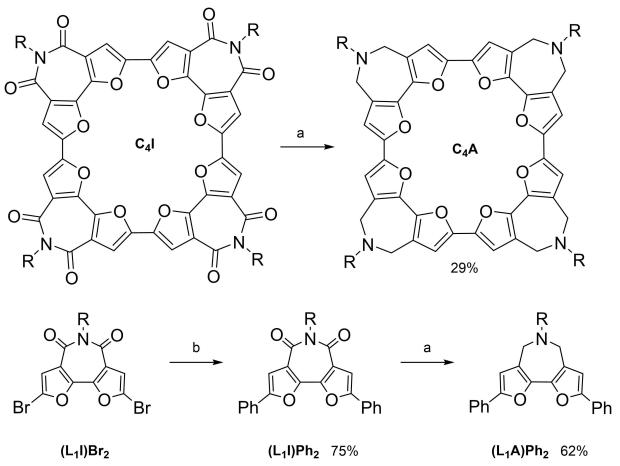

Scheme 2. Synthesis of **C$_4$A** and **(L$_1$A)Ph$_2$**. Conditions: (a) $LiAlH_4$, THF, 0 °C→ rt, dark; (b) $Pd(PPh_3)_4$, toluene-water (2:1), 100 °C, 20 h. R = 2-octyldodecyl.

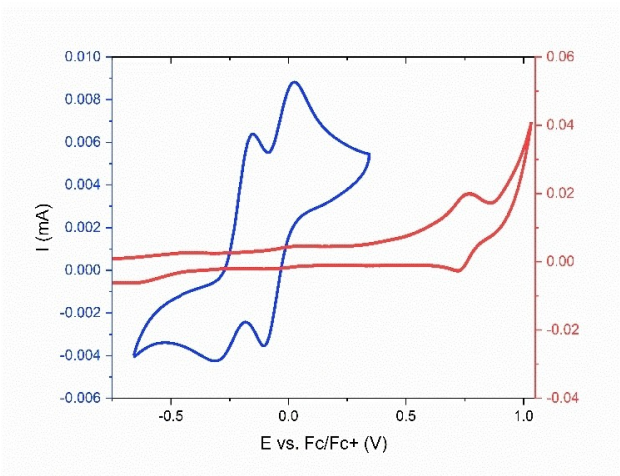

Figure 1. Cyclic voltammetry of **C_4A** (blue) and **C_4I** (red) in dichloromethane as a solvent and 0.1 M (nBu)$_4$NClO$_4$ (TBAPC) as an electrolyte, referenced against the Fc/Fc$^+$ redox couple (the scan rate was 100 mV/s).

than the values reported for tetrathiafulvalene oligopyrrole macrocycles.[41,42]

Electron density maps revealed that reducing the carbonyl groups in **C_4I** causes the electron density to shift towards the interior of the macrocycle, thus increasing the overall electron density in the cavity (Figure 2). Nevertheless, addition of different guest molecules did not result in complexation. The calculated HOMO–LUMO gap is nearly identical for **C_4A** and **C_4I** (2.38 eV and 2.39 eV, respectively), and a similar observation can be made for the linear oligomers, **L_4A** and **L_4I** (Table S4, see Supporting Information). For the macrocycle, replacing the carbonyl groups with methylene causes the energies of both HOMO and LUMO to increase by approximately 1.8 eV, whereas for the linear oligomers, this effect is slightly less pronounced, with an increase of approximately 1.6 eV.

The absorption spectrum of **C_4A** reveals a band at 394 nm, which corresponds to the $S_0 \rightarrow S_n$ ($n > 1$) transition, as well as very weak absorption band in the 415–550 nm range, which we assign to the symmetry-forbidden $S_0 \rightarrow S_1$ transition (Figure 3a, blue trace). Unlike **C_4I**, which displays weak, yet observable emission, no emission was observed for **C_4A**. Indeed, in the absorption spectra for **C_4I** (Figure 3a, red trace), the intensity of

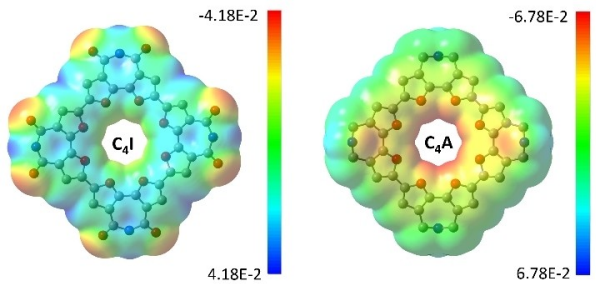

Figure 2. Electron density maps for **C_4I** (left) and **C_4A** (right) calculated at the DFT/B3LYP/6-311G(d) level of theory.

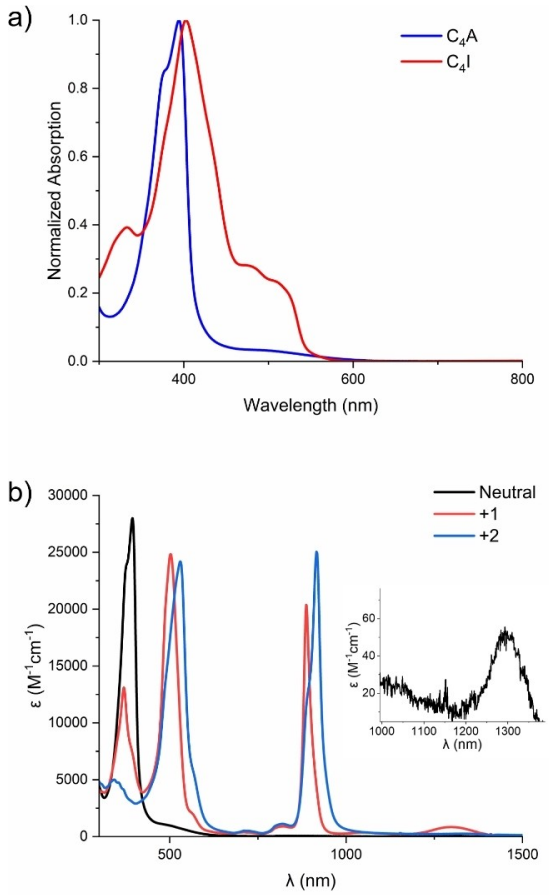

Figure 3. (a) Normalized absorption spectra of **C_4A** (blue) and **C_4I** (red) measured in $CHCl_3$. The forbbiden $S_0 \rightarrow S_1$ transition is less pronounced for **C_4A**. (b) Absorption spectra of **C_4A** (black), **C_4A$^{\bullet+}$** (red), and **C_4A^{2+}** (blue) measured in chloroform and NO•SbF_6 as an oxidant. Inset: The expansion of the absorption spectra of **C_4A** before the addition of an oxidant at 1000–1400 nm.

the $S_0 \rightarrow S_1$ band is 24% of the $S_0 \rightarrow S_n$ band; while for **C_4A** the intensity of $S_0 \rightarrow S_1$ is lower than 3%, compared with $S_0 \rightarrow S_n$. A possible explanation for this difference might stem from the higher electron density of the π-conjugated backbone of **C_4A**, which increases its quinoid character. The resulting rigid backbone is therefore distorted to a lesser extent, which is expressed by a lower oscillator strength for the Laporte-forbidden $S_0 \rightarrow S_1$ and $S_1 \rightarrow S_0$ transitions.

Upon oxidation using NO•SbF_6, a solution of **C_4A** changes from pale yellow to deep red and three additional bands emerge: two sharp bands at 500 nm and 887 nm, and a weak, broad band at 1300 nm, all of which we assigned to the radical cation, **C_4A$^{\bullet+}$** (Figure 3b, red). Even with the absence of an oxidant, a weak absorption peak is observable at 1300 nm (Figure 3b, inset), which disappears with the addition of a reducer such as $NaBH_4$. This further validates the ease of the oxidation of **C_4A**, which is partially oxidized under ambient conditions. It is interesting to compare these spectra with those of **C_{10}T** dication, which displays similar features but is bathochromically shifted, with two bands at 683 nm and 1334 nm.[24]

The addition of hydrazine hydrate solution to the dication solution of **C_4A** restores the spectrum to that of the neutral macrocycle, indicating that this chemical oxidation is fully reversible. The ease of oxidation was also demonstrated by two-electron oxidation with TCNQ-F_4, resulting in spectra similar to those observed with inorganic oxidants (Figure S27, see Supporting Information).

The EPR measurements of **C_4A** were performed by applying external voltage to oxidize the macrocycle in a solution containing 0.1 M $(n\text{Bu})_4\text{NClO}_4$ (TBAPC) in dichloromethane (Figure 4). When a potential of −0.21 V is applied, a signal emerges that is assigned to the cation radical (**$C_4A^{\bullet+}$**); the lack of hyperfine coupling observed indicates strong delocalization of the electron along the macrocycle. Upon increasing the potential past the second oxidation wave, this signal vanishes, clearly indicating the formation of the dication.

Compared with its slightly larger thiophene analog, **C_{10}T**,[24] **C_4A** exhibits different behavior. Two electron oxidation in **C_{10}T** results in polaron pair, as indicated by both active EPR signal

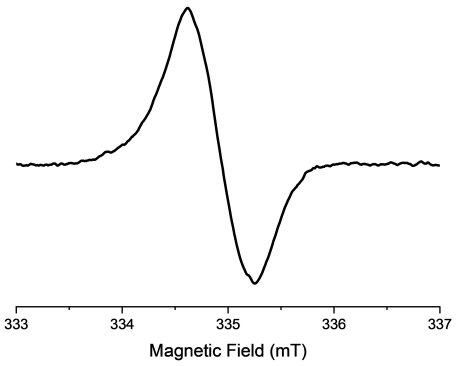

Figure 4. EPR spectrum of **C_4A** measured in a solution of 0.1 M tetrabutyl ammonium perchlorate (TBAPC) in dichloromethane with a potential of −0.21 V vs. an Ag/AgCl reference electrode, with a sweep range of 5 mT and a field modulation of 5 μT. The lack of hyperfine coupling indicates very strong delocalization of the electron along the macrocycle; the spectrum is attributed to the radical cation (**$C_4A^{\bullet+}$**).

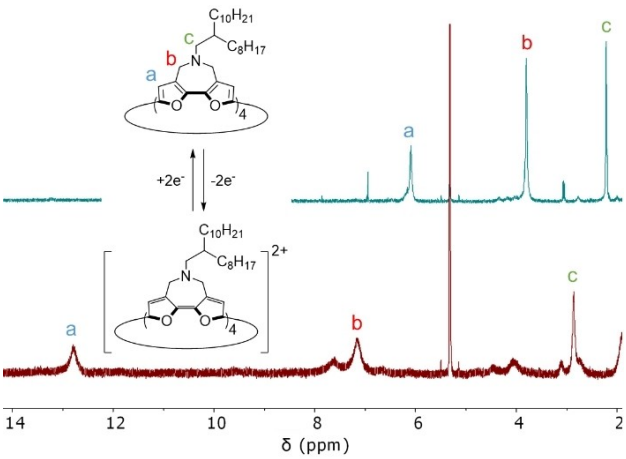

Figure 5. ^{1}H NMR spectra of **C_4A** (top) and **C_4A^{2+}** (bottom) in CD_2Cl_2 measured at 273 K.

and absorbance bands in the NIR region. In contrast, the lack of an EPR signal combined with the lack of transitions in the NIR region, indicates that **C_4A^{2+}** has a bipolaronic nature. This is in line with the smaller size and higher quinoid character of **C_4A**, since the existence of a polaron pair requires a structural distortion, to allow the confinement of two separated polarons.

Since **C_4A** consists of accessible oxidation states, we studied the switching of the magnetic ring currents from the neutral state (4nπ electrons) to the dication state ((4n+2)π electrons). The addition of $AgSbF_6$ to a solution of **C_4A** in CD_2Cl_2 at 0 °C resulted in a deep purple solution with a resolved ^{1}H NMR spectrum corresponding to **C_4A^{2+}** (Figure 5, bottom). The ß-protons (*a*) experience a significant downfield shift from 6.1 to 12.8 ppm. It is interesting that even distant protons, separated from the π-system by one or more sp^3 carbons, are also significantly affected by the diatropic global current: the methylene protons (*b*) experience a downfieldshift from 4 ppm to 7.1 ppm, and even the N-methylene protons (*c*), which are four sp^3 bonds apart from the π-conjugated backbone, are affected, with a downfield shift from 2.1 ppm to 2.9 ppm.

To verify that the changes in the chemical shifts stem from the global aromatic character of the dication rather than from decreased shielding induced by the removal of two electrons, we compared the calculated chemical shifts of both the cyclic and linear oligomers (DFT/ωB97XD/6-311G(d)).[43] We found that the calculated chemical shift for the ß-protons of **C_4A** increases by 7.17 ppm upon oxidation (from 5.67 ppm for **C_4A** to 12.84 ppm for **C_4A^{2+}**), which is in line with the abovementioned trend observed in the experimental spectum. In contrast, the 2-electron oxidation of the linear oligomer **L_4A** results in only a mild downfield shift of the inner-most ß-protons by 0.83 ppm (from 6.24 ppm in the neutral state to 7.07 ppm for the dicaton). The differences clearly suggest that the change in the chemical shifts upon oxidation mainly results from the global ring currents.

The reduction of the electron-withdrawing carbonyl groups to methylenes increases the electron density in the π-conjugated backbone, which should be expressed in the global anti-aromatic ring current. Indeed, the ß-protons experience an upfield shift from 7.35 ppm for **C_4I** to 6.04 ppm for **C_4A**. The difference of 1.31 ppm can stem from either an increase in the global paratropic ring current or from an increase in the electron density of methylene vs. carbonyl. To better understand the impact of these two contributors, we compared a non-cyclic bifuranimide and bifuran-amine units capped with two phenyls (**(L_1A)Ph_2** and **(L_1I)Ph_2**). The smaller difference in the chemical shift of 0.85 ppm (7.41 for **(L_1I)Ph_2** vs. 6.56 ppm **(L_1A)Ph_2**)) in the ß-protons indicates that the increase in the global paratropic current is a major contributor.

To corroborate these findings, we evaluated the extent of the global effects by employing two computational tools: Nuclear independent chemical shifts (NICS)[44] and anisotropy of the current (induced) density (ACID).[45,46] $NICS(1)_{zz}$ probes the ring current 1 Å above the center of the ring in question; negative values indicate a diatropic ring current (an aromatic system), whereas positive values suggest a paratropic ring current (an antiaromatic system). To evaluate the contribution

of the local and global aromatic ring currents, we calculated the NICS(1)$_{zz}$ values for each furan ring in both **C$_4$A** and **L$_4$A**. Since furan itself is aromatic, with a NICS(1)$_{zz}$ value of −27.1 ppm (calculated in the same level of theory), this value should increase when furans constitute a 4nπe$^-$ macrocycle, and decrease in (4n+2)πe$^-$ macrocycle. Indeed, upon oxidation of **C$_4$A** to **C$_4$A^{2+}**, the NICS(1)$_{zz}$ value decreases by 11 ppm, from −8 to −19 ppm, respectively. In contrast, oxidation of the linear tetramer, **L$_4$A**, to **L$_4$A^{2+}** had almost no effect on the NICS(1)$_{zz}$ values, which slightly increase from −7.5 ppm to −7 ppm. This indicates that this NICS(1)$_{zz}$ is strongly affected by a switch of the global ring current. Figure 6 presents NICS$_{zz}$ maps for **C$_4$A** (a) and **C$_4$A^{2+}** (b); blue and red denote negative and positive chemical shifts, corresponding to diatropic and paratropic currents, respectively. For the neutral molecules, the furan rings are aromatic, whereas the interior of the macrocycle is slightly antiaromatic. Upon two-electron oxidation, the aromaticity of the furan rings increases significantly, and they no longer appear as individual rings with local current, this indicates an increasing global influence for the case of **C$_4$A^{2+}**. In addition, the interior of the macrocycle switches from antiaromatic to aromatic, as expected for a 30πe$^-$ backbone.

ACID plots employ surfaces (yellow) and vectors (green) to indicate the current density and direction as a method of quantifying π-conjugation, delocalization, and the aromaticity of conjugated systems.[46] The surfaces indicate the pathways along which the currents are delocalized, and the vectors can indicate aromaticity (clockwise, diatropic ring current), antiaromaticity (anti-clockwise, paratropic ring current) or their lack thereof. The ACID plot of **C$_4$A** shows a global paratropic ring current delocalized along the C$_\alpha$-C$_\alpha$-O pathway that is in accordance with the antiaromaticity of the neutral macrocycle, as suggested by the NICS calculations (Figure 6c, d). Upon oxidation to the cation, the current density along the C$_\alpha$-C$_\beta$-C$_\beta$-C$_\alpha$ pathway increases to match that of the C$_\alpha$-C$_\alpha$-O pathway inside the furans; the global ring current shifts to a diatropic ring current. Upon oxidation to the dication, the current density is more prominently shifted to the C$_\alpha$-C$_\beta$-C$_\beta$-C$_\alpha$ pathway and the diatropic ring current becomes more pronounced (see Figures S38-40 in the Supporting Information).

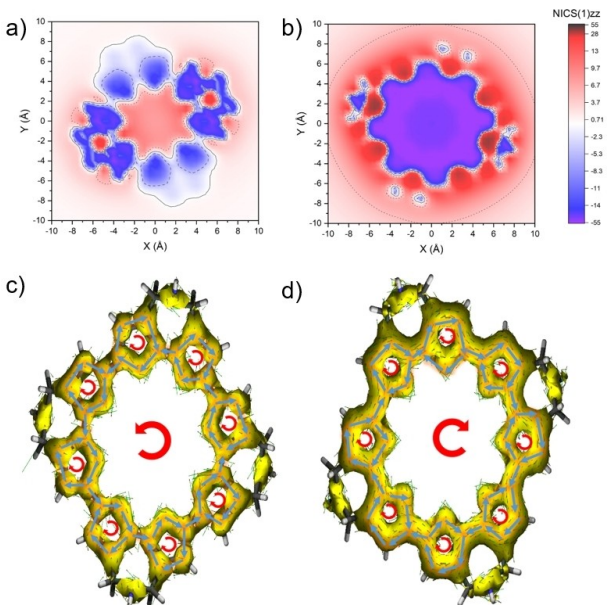

Figure 6. NICS$_{zz}$ plots at the z=1 plane for (a) **C$_4$A** and (b) **C$_4$A^{2+}** and ACID plots for (c) **C$_4$A** and (d) **C$_4$A^{2+}** calculated at the DFT/ωB97XD/6-311G(d) level of theory.

Conclusions

In summary, using a post-synthetic approach, we introduced the first macrocyclic furan with accessible oxidation states. The high HOMO level is manifested in the ease of oxidation, with an E_{ox}^1 value of −0.23 vs. that of Fc/Fc$^+$, and the macrocycle is partially oxidized under ambient conditions, as indicated from a weak absorption band observed at 1300 nm. To the best of our knowledge, such low oxidation potential is unprecedented in π-conjugated macrocycles. Upon oxidation, the globally-antiaromatic backbone (32πe$^-$) switches to a global aromatic state (30πe$^-$), as manifested by the formation of a strong diatropic current observed in the ^{1}H NMR spectrum. NICS and ACID calculations support this trend, and provide evidence for different pathways for the global current in the neutral and dicationic states. The combination of absorption and EPR spectroscopies indicated that **C$_4$A^{2+}** exists as a bipolaron rather than polaron pair, which can be explained by its highly planar and rigid backbone. The potential of furan macrocycles as strong p-type material, as well as precursor for the synthesis of cycloparaphenylenes,[47] is currently being studied in our group.

Acknowledgements

This research was supported by the European Research Council (ERC) under the European Union's Horizon 2020 research and innovation program (Grant Agreement No. 850836, ERC Starting Grant "PolyHelix"). This research was supported by The Israel Science Foundation – FIRST Program (grant No. 1453/19).

Conflict of Interest

The authors declare no conflict of interest.

Data Availability Statement

The data that support the findings of this study are available in the Supporting Information.

Keywords: π-conjugated macrocycles · aromaticity · macrocyclic compounds · oligofurans · organic semiconductors

[1] M. Iyoda, J. Yamakawa, M. J. Rahman, *Angew. Chem. Int. Ed.* **2011**, *50*, 10522–10553; *Angew. Chem.* **2011**, *123*, 10708–10740.

[2] Y. Xu, R. Kaur, B. Wang, M. B. Minameyer, S. Gsänger, B. Meyer, T. Drewello, D. M. Guldi, M. von Delius, *J. Am. Chem. Soc.* **2018**, *140*, 13413–13420.
[3] J. D. Cojal González, M. Iyoda, J. P. Rabe, *Angew. Chem. Int. Ed.* **2018**, *57*, 17038–17042; *Angew. Chem.* **2018**, *130*, 17284–17288.
[4] Y. Zhong, Y. Yang, Y. Shen, W. Xu, Q. Wang, A. L. Connor, X. Zhou, L. He, X. C. Zeng, Z. Shao, Z. Lu, B. Gong, *J. Am. Chem. Soc.* **2017**, *139*, 15950–15957.
[5] D. Lorbach, A. Keerthi, T. M. Figueira-Duarte, M. Baumgarten, M. Wagner, K. Müllen, *Angew. Chem. Int. Ed.* **2016**, *55*, 418–421; *Angew. Chem.* **2016**, *128*, 427–431.
[6] H. Gregolińska, M. Majewski, P. J. Chmielewski, J. Gregoliński, A. Chien, J. Zhou, Y.-L. Wu, Y. J. Bae, M. R. Wasielewski, P. M. Zimmerman, M. Stępień, *J. Am. Chem. Soc.* **2018**, *140*, 14474–14480.
[7] M. Stępień, E. Gońka, M. Żyła, N. Sprutta, *Chem. Rev.* **2017**, *117*, 3479–3716.
[8] J. M. W. Chan, J. R. Tischler, S. E. Kooi, V. Bulović, T. M. Swager, *J. Am. Chem. Soc.* **2009**, *131*, 5659–5666.
[9] S. Eder, D.-J. Yoo, W. Nogala, M. Pletzer, A. Santana Bonilla, A. J. P. White, K. E. Jelfs, M. Heeney, J. W. Choi, F. Glöcklhofer, *Angew. Chem. Int. Ed.* **2020**, *59*, 12958–12964; *Angew. Chem.* **2020**, *132*, 13058–13064.
[10] J. L. Sessler, D. Seidel, *Angew. Chem. Int. Ed.* **2003**, *42*, 5134–5175; *Angew. Chem.* **2003**, *115*, 5292–5333.
[11] C. Liu, Y. Ni, X. Lu, G. Li, J. Wu, *Acc. Chem. Res.* **2019**, *52*, 2309–2321.
[12] E. Vogel, N. Jux, J. Dörr, T. Pelster, T. Berg, H.-S. Böhm, F. Behrens, J. Lex, D. Bremm, G. Hohlneicher, *Angew. Chem. Int. Ed.* **2000**, *39*, 1101–1105; *Angew. Chem.* **2000**, *112*, 1143–1147.
[13] E. Vogel, M. Sicken, P. Röhrig, H. Schmickler, J. Lex, O. Ermer, *Angew. Chem. Int. Ed.* **1988**, *27*, 411–414; *Angew. Chem.* **1988**, *100*, 450–453.
[14] M. D. Peeks, M. Jirasek, T. D. W. Claridge, H. L. Anderson, *Angew. Chem. Int. Ed.* **2019**, *58*, 15717–15720; *Angew. Chem.* **2019**, *131*, 15864–15867.
[15] M. Rickhaus, M. Jirasek, L. Tejerina, H. Gotfredsen, M. D. Peeks, R. Haver, H.-W. Jiang, T. D. W. Claridge, H. L. Anderson, *Nat. Chem.* **2020**, *12*, 236–241.
[16] H. Ogawa, C. Fukuda, T. Imoto, I. Miyamoto, T. Taniguchi, T. Koga, Y. Nogami, *Tetrahedron Lett.* **1983**, *24*, 1045–1048.
[17] J. S. Wössner, D. Wassy, A. Weber, M. Bovenkerk, M. Hermann, M. Schmidt, B. Esser, *J. Am. Chem. Soc.* **2021**, *143*, 12244–12252.
[18] H. Shimizu, J. D. Cojal González, M. Hasegawa, T. Nishinaga, T. Haque, M. Takase, H. Otani, J. P. Rabe, M. Iyoda, *J. Am. Chem. Soc.* **2015**, *137*, 3877–3885.
[19] M. Williams-Harry, A. Bhaskar, G. Ramakrishna, T. Goodson, M. Imamura, A. Mawatari, K. Nakao, H. Enozawa, T. Nishinaga, M. Iyoda, *J. Am. Chem. Soc.* **2008**, *130*, 3252–3253.
[20] K. Nakao, M. Nishimura, T. Tamachi, Y. Kuwatani, H. Miyasaka, T. Nishinaga, M. Iyoda, *J. Am. Chem. Soc.* **2006**, *128*, 16740–16747.
[21] F. Zhang, G. Götz, H. D. F. Winkler, C. A. Schalley, P. Bäuerle, *Angew. Chem. Int. Ed.* **2009**, *48*, 6632–6635; *Angew. Chem.* **2009**, *121*, 6758–6762.
[22] J. Fabian, H. Hartmann, *J. Phys. Org. Chem.* **2007**, *20*, 554–567.
[23] G. Fuhrmann, T. Debaerdemaeker, P. Bäuerle, *Chem. Commun.* **2003**, 948–949.
[24] F. Zhang, G. Gotz, E. Mena-Osteritz, M. Weil, B. Sarkar, W. Kaim, P. Bauerle, *Chem. Sci.* **2011**, *2*, 781–784.
[25] J. Krömer, I. Rios-Carreras, G. Fuhrmann, C. Musch, M. Wunderlin, T. Debaerdemaeker, E. Mena-Osteritz, P. Bäuerle, *Angew. Chem. Int. Ed.* **2000**, *39*, 3481–3486; *Angew. Chem.* **2000**, *112*, 3623–3628.
[26] O. Dishi, O. Gidron, *J. Org. Chem.* **2018**, *83*, 3119–3125.
[27] O. Gidron, Y. Diskin-Posner, M. Bendikov, *J. Am. Chem. Soc.* **2010**, *132*, 2148–2150.
[28] O. Gidron, M. Bendikov, *Angew. Chem. Int. Ed.* **2014**, *53*, 2546–2555; *Angew. Chem.* **2014**, *126*, 2580–2589.
[29] O. Gidron, A. Dadvand, Y. Sheynin, M. Bendikov, D. F. Perepichka, *Chem. Commun.* **2011**, *47*, 1976–1978.
[30] A. Hayoun Barak, G. de Ruiter, M. Lahav, S. Sharma, O. Gidron, G. Evmenenko, P. Dutta, M. Bendikov, M. E. van der Boom, *Chem. Eur. J.* **2013**, *19*, 8821–8831.
[31] S. V. Mulay, B. Bogoslavky, I. Galanti, E. Galun, O. Gidron, *J. Mater. Chem. C* **2018**, *6*, 11951–11955.
[32] S. V. Mulay, O. Dishi, Y. Fang, M. R. Niazi, L. J. W. Shimon, D. F. Perepichka, O. Gidron, *Chem. Sci.* **2019**, *10*, 8527–8532.
[33] O. Dishi, P. Malakar, L. J. W. Shimon, S. Ruhman, O. Gidron, *Chem. Eur. J.* **2021**, *27*, 17794–17801.
[34] A. J. Varni, M. Kawakami, S. A. Tristram-Nagle, D. Yaron, T. Kowalewski, K. J. T. Noonan, *Org. Chem. Front.* **2021**, *8*, 1775–1782.
[35] T. Köhler, Z. Ou, J. T. Lee, D. Seidel, V. Lynch, K. M. Kadish, J. L. Sessler, *Angew. Chem. Int. Ed.* **2005**, *44*, 83–87; *Angew. Chem.* **2005**, *117*, 85–89.
[36] K. Kupietz, M. J. Białek, B. Szyszko, A. Sarwa, L. Latos-Grażyński, *Org. Chem. Front.* **2022**, *9*, 2968–2976.
[37] M. O. Senge, *Chem. Commun.* **2011**, *47*, 1943–1960.
[38] F. Feixas, E. Matito, J. Poater, M. Solà, *Chem. Soc. Rev.* **2015**, *44*, 6434–6451.
[39] M. Iyoda, K. Tanaka, H. Shimizu, M. Hasegawa, T. Nishinaga, T. Nishiuchi, Y. Kunugi, T. Ishida, H. Otani, H. Sato, K. Inukai, K. Tahara, Y. Tobe, *J. Am. Chem. Soc.* **2014**, *136*, 2389–2396.
[40] S. Akoudad, P. Frère, N. Mercier, J. Roncali, *J. Org. Chem.* **1999**, *64*, 4267–4272.
[41] F. Zhang, G. Götz, H. D. F. Winkler, C. A. Schalley, P. Bäuerle, *Angew. Chem. Int. Ed.* **2009**, *48*, 6632–6635; *Angew. Chem.* **2009**, *121*, 6758–6762.
[42] A. Jana, M. Ishida, J. S. Park, S. Bähring, J. O. Jeppesen, J. L. Sessler, *Chem. Rev.* **2017**, *117*, 2641–2710.
[43] Against TMS reference (B3LYP/6-311 + g(2d, GIAO) in GaussView6,.
[44] Z. Chen, C. S. Wannere, C. Corminboeuf, R. Puchta, P. von R. Schleyer, *Chem. Rev.* **2005**, *105*, 3842–3888.
[45] R. Herges, D. Geuenich, *J. Phys. Chem. A* **2001**, *105*, 3214–3220.
[46] D. Geuenich, K. Hess, F. Köhler, R. Herges, *Chem. Rev.* **2005**, *105*, 3758–3772.
[47] S. Gadakh, L. J. W. Shimon, O. Gidron, *Angew. Chem. Int. Ed.* **2017**, *56*, 13601–13605; *Angew. Chem.* **2017**, *129*, 13789–13793.

Manuscript received: July 4, 2022
Accepted manuscript online: August 5, 2022
Version of record online: September 2, 2022